



Formation of snowflake-like CdS/reduced graphene oxide composite for efficient photocatalytic organic dye degradation

Huhu Gao¹ · Zunli Mo¹ · Ruibin Guo¹ · Xiaohui Niu¹ · Zhenliang Li¹

Received: 5 October 2017 / Accepted: 8 January 2018 / Published online: 19 January 2018
© Springer Science+Business Media, LLC, part of Springer Nature 2018

Abstract

Photocatalytic efficiency of CdS can be improved significantly by controlling the morphology and recombining with other semiconductor materials. In this work, a novel snowflake-like CdS/reduced graphene oxide (rGO) composite was prepared by a simple hydrothermal process using graphene oxide and CdS as raw materials and L-aspartic acid as template. The structure of the composites were characterized by scanning electron microscopy, transmission electron microscopy, X-ray diffraction. Through a basic analysis, a simple synthesis mechanism of snowflake-like CdS is proposed, and transient photocurrent technology demonstrate that the photocurrent of snowflake-like CdS/rGO is greatly improved. Compared with pure CdS, snowflake-like CdS/rGO exhibits efficient organic dye adsorption and degradation under visible light irradiation, resulting from the involving of rGO sheet as chainmail, which facilitates the charge separation, suppresses the recombination of electron–hole pairs, and improves light conversion efficiency of catalysts.

1 Introduction

Morphology-controlled synthesis of 3D hierarchical nano-/micro-crystals has been extensively studied in the past decades owing to their unique structure-dependent properties, wide applications in fields such as environmental purification, biomedical fields and solar energy conversion, which has been a challenging but significant research topic due to growing environmental concerns and increasing energy demand [1–4]. As mean to achieve this goal, a variety of photocatalysts have been extensively studied, Especially, The 3D hierarchical nano-/micro-crystals, which can not only reserve the unique nanometer-scaled properties but also overcome their shortcomings of difficult separation

and poor stability. CdS is probably one of the most studied metal sulfide materials with a direct band gap of 2.42 eV [5], which corresponds well with the solar spectrum and shows the potential in the field of nonlinear optics and photocatalysis. Therefore, synthesis of a CdS micro-/nano-crystals with special morphology to enhance its photoelectric activity is particularly important [6]. The polymer-assisted method has been widely used in the preparation of different micro-nanostructured materials in recent years, especially biomolecules, due to its unique structure and attractive self-assembly function make them to serve as templates for designing and fabricating many functional composites [7, 8]. Wu et al. synthesis a variety of multi-shelled hollow spheres by adding different organic molecules [9, 10]. Among many biomolecules, amino acids can help semiconductors to synthesize complex three-dimensional structures by using its unique functional groups. Wu et al. has reported a facile histidine assisted method for synthesis of ZnO hierarchical architectures [11]. However, prolonged irradiation of CdS suspensions leads to photocorrosion still limit its further applications [12]. Fortunately, CdS has a unique band structure, so it can be combined with other materials to form heterojunction semiconductors [13–15], which will greatly improving its stability and photocatalytic efficiency. For example, the structures composed of CdS and other semiconductors (CTNs, TiO₂, etc) have been synthesised and used for photocatalytic systems [16].

Electronic supplementary material The online version of this article (<https://doi.org/10.1007/s10854-018-8567-5>) contains supplementary material, which is available to authorized users.

✉ Zunli Mo
mozlnwnu2010@163.com

✉ Ruibin Guo
nwnugrb@163.com

¹ Key Laboratory of Eco-Environment-Related Polymer Materials, Ministry of Education of China, and Key Laboratory of Polymer Materials of Gansu Province, College of Chemistry and Chemical Engineering, Northwest Normal University, Lanzhou 730070, People's Republic of China

As an ultrathin two-dimensional material, graphene possesses many exciting properties, such as broad band gap and electron conduction ability [17, 18]. Despite its many advantages, loading graphene nanosheets indirectly onto the surface of semiconductor nanomaterials is difficult. A number of reports have indicated that GO has many functional groups containing oxygen. Compared with graphene, GO can be well compounded with other semiconductor materials [19]. And the composites material will have more excellent photoelectric properties by further reducing the graphene oxide in the catalyst preparation process [20–22]. To the best of our knowledge, using a biomolecule-assisted methods to fabricate three-dimensional snowflake-like CdS/reduced graphene oxide (rGO) composite photocatalysts with chemically cross-linked semiconductor and graphitic carbon bonding to improve the sunlight stability was rarely reported before.

Herein, we report the synthesis of a novel 3D snowflake-like CdS–rGO (3D CdS–rGO) nanocomposites where rGO sheets is well supported on a snowflake-like CdS surface. L-Aspartic acid and temperature is found to significantly influence the morphologies of CdS crystals and the experiment on photocatalytic degradation of rhodamin B (RhB) aqueous solution shows that the as-prepared 3D snowflake-like CdS–rGO display much enhanced photocatalytic performance under simulated sunlight irradiation.

2 Experimental

2.1 Materials

Potassium permanganate (KMnO_4) was obtained from Dan Dong No. 1 Chemical Plant. Glycol, hydrogen peroxide (H_2O_2), phosphoric acid (H_3PO_4), L-aspartic acid and RhB were purchased from China National Pharmaceutical Group. Sulfuric acid (H_2SO_4) and hydrochloric acid (HCl) were bought from BaiYin LiangYou Chemical Reagents Co., Ltd. Graphite powder and Cadmium acetate was supplied by Aladdin Industrial Corporation Shanghai (China). Thiourea was purchased from Tianjin Kay Tong Chemical Reagent Co., Ltd. Sodium sulfide was purchased from Shanghai Tongya Chemical Technology Development Co., Ltd. All chemicals were of analytic grade and used as received. The deionized water used in the experiment was purified by tap water.

2.2 Preparation of GO

GO was synthesized from graphite powder (100 mesh) by using a modified Hummers method [23, 24]. In brief, 1.5 g of graphite powder was mixed with 6.0 g of KMnO_4 , and then put slowly into 200 mL beaker containing of a mixture

H_2SO_4 and H_3PO_4 (volume ratio of $\text{H}_2\text{SO}_4:\text{H}_3\text{PO}_4=9:1$) under vigorous stirring while the temperature was kept below $10\text{ }^\circ\text{C}$. 1 h later, The mixture was stirred in the ice bath for 2 h and stirred at $35\text{ }^\circ\text{C}$ in a water bath for another 0.5 h. After that, the mixture was poured into 400 mL of ice deionized water containing 10 mL of 30% H_2O_2 to remove the excess KMnO_4 , and the colour of mixture turned bright yellow immediately. Then, the reaction mixture was washed in succession with 5% HCl, deionized water and ethanol till the pH value increased to 5–6. Finally, the resulting solid was dried at $60\text{ }^\circ\text{C}$ in a vacuum oven for 12 h.

2.3 Preparation of catalysts

The 3D snowflake-like CdS were synthesized by a hydrothermal method. In a typical procedure, 1 mmol of $\text{Cd}(\text{C}_2\text{H}_3\text{O}_2)_2 \cdot 2\text{H}_2\text{O}$, 3 mmol of thiourea, and 0.2 mmol of L-aspartic acid were dispersed in 30 mL distilled water. After vigorous stirring and sonication, The precursor solution was transferred into a 50 mL Teflon-lined autoclave and held at $180\text{ }^\circ\text{C}$ for 4 h. Then cooling to room temperature, the precipitates were filtered and rinsed several times with distilled water and ethanol several times, dried in a vacuum oven at $60\text{ }^\circ\text{C}$ for 12 h. For the synthesis of 3D CdS–rGO nanocomposites, different amount of GO that was prepared via the modified hummer method were dispersed in the mixture of 30 mL glycol and 10 mL water follow by ultrasonication for 120 min. Then 3D snowflake-like CdS was added to the GO dispersion and the suspension continue to ultrasonicate for few minutes. Resultant suspension was sealed in a Teflon-lined autoclave and held at $160\text{ }^\circ\text{C}$ for 4 h. The final product filtered and rinsed several times with distilled water and ethanol several times, dried in a vacuum oven at $60\text{ }^\circ\text{C}$. The 3D CdS–rGO nanocomposites with different amount of rGO are denoted as 3D CdS–rGO (x wt%). For synthesis of pure CdS, in a typical procedure, 1 mmol of $\text{Cd}(\text{C}_2\text{H}_3\text{O}_2)_2 \cdot 2\text{H}_2\text{O}$, and 3 mmol of $\text{Na}_2\text{S} \cdot 9\text{H}_2\text{O}$ were dispersed in 50 mL distilled water. Next, the solution was stirred vigorously at room temperature for 6 h. After that, the precipitates were collected by centrifugation and washed with distilled water and ethanol several times. The final product was dried in a vacuum oven at $60\text{ }^\circ\text{C}$ for 12 h.

2.4 Characterization of catalysts

The morphology of the samples was obtained by a field emission scanning electron microscopy (SEM) and transmission electron microscope (TEM, USA FEI Tecnai G²TF20) operating at 200 kV. The photocatalysts were supported on a carbon film coated on fine mesh copper grid. Samples were ultrasonicated in ethanol and a drop was dripped on the support film. Crystallographic structures of samples were examined by X-ray diffraction

(XRD) measurements using a D/Max-2400 powder diffractometer with Cu K α X ray sources (Japanese Physical Company) at 40 kV and 40 mA in the 2θ range of 5° – 70° , with a scan rate of 0.02° per second. The IR analyses were carried out on a FTIR Analyzer (EQUINOX55) using KBr pellet method in the range of 400 – 4000 cm^{-1} . UV–vis diffuse reflectance spectroscopy (DRS) in the UV/vis region was measured on a Shimadzu UV-2550 spectrophotometer equipped with an integrating sphere, BaSO $_4$ was used as a reflectance standard.

2.5 Photoelectrochemical measurements

The transient photocurrent responses systems were composed of a CHI660E electrochemistry potentiostat (Shanghai Chenhua Limited, China), with a 100 W tungsten filament lamp and a homemade three-electrode cell using Pt wire as the counter electrode and Hg/HgCl as reference electrode, and 0.5M Na $_2$ SO $_4$ as electrolyte. Specifically, Pure CdS, 3D CdS–rGO, and flower-like CdS electrodes were prepared by depositing suspensions made of the corresponding sample and absolute ethanol (the concentration of samples are 1.0 g/L) onto FTO conducting glass (1×1 cm^2), then dried in a vacuum oven at 60°C for 3 h to be tested.

2.6 Photocatalytic degradation

The adsorptive and photocatalytic performance of the catalyst were evaluated by measuring the adsorption and photocatalytic degradation of RhB from aqueous solution under atmosphere. The photocatalytic reaction of samples were carried out in photocatalytic reactor (see Fig. S1), a 300 W Xe arc lamp was applied for light source, and the temperature of the reaction system was maintained at room temperature by passing cooling water. Specifically, 50 mg of 3D CdS–rGO and RhB (50 mL, 2.5×10^{-5} mol/L) placed in a quartz well in an optical system comprising a 300 W Xe lamp with a 420 nm cut-off filter. Before irradiation, the suspensions were magnetically stirred in the dark for 1.5 h to ensure the establishment of an adsorption/desorption equilibrium between the organic species and the catalyst. At a given exposure time interval, 5 mL solution was collected, centrifuged, and then filtered through a Millipore filter to remove the catalyst particulates. Finally, the concentration change of RhB was determined by measuring the maximum absorbance at 552 nm using a UV–vis spectrophotometer. For comparison, we also tested the photocatalytic activities of pure CdS, and snowflake-like CdS under the same experimental conditions.

3 Results and discussion

Powder XRD analysis is used to investigate the phase structure and crystalline size of the material. Figure 1. presents the XRD patterns of GO, snowflake-like CdS and 3D CdS–rGO nanocomposites. The diffraction peaks of snowflake-like CdS match well with the theoretical values of the hexagonal structure of CdS (JCPDS No: 41-1049) with the lattice parameters $\alpha = 4.140^\circ$. The feature peak of GO is at around $2\theta = 9.8^\circ$, corresponding to the (002) plane with an interlayer spacing of 0.90 nm, indicating that the oxygen-containing functional groups induced between GO sheets by the modified Hummers method, causing the increasing of interlayer spacing. In addition, both snowflake-like CdS and 3D CdS–rGO exhibit similar diffraction peaks and intensities without any considerable change. The characteristic peak of GO vanishes, which might be attributed to the reduction of GO and the destruction of regular stack of GO sheets during hydrothermal processes [25].

To better understand the formation of snowflake-like CdS structures, we conducted a series of controlled experiments by changing the experimental parameters, and the morphology of the as-synthesized snowflake-like CdS and 3D CdS–rGO was examined by SEM. At first, the concentration-dependent images of the synthesized products were studied. Figure 2a shows the images of irregularity agglomeration architecture of CdS prepared without L-aspartic acid. And it is interesting to find from Fig. 2b that the morphology of CdS changed from spherical accumulation to cauliflower when the amount of L-aspartic acid was 1 mmol. As the amount of L-aspartic acid was increased to 2 mmol, the morphology changes from cauliflower-like shape to regular snowflake structure consisted of CdS nanospheres. (Fig. 2c, d), which protrude from the root of the snowflake-like CdS. With the amount of L-aspartic acid increased to 4 and

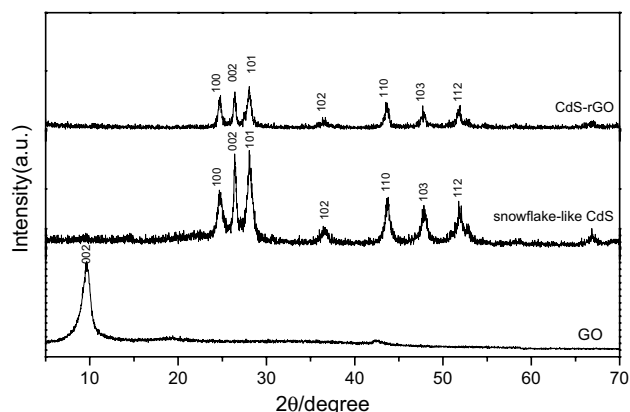
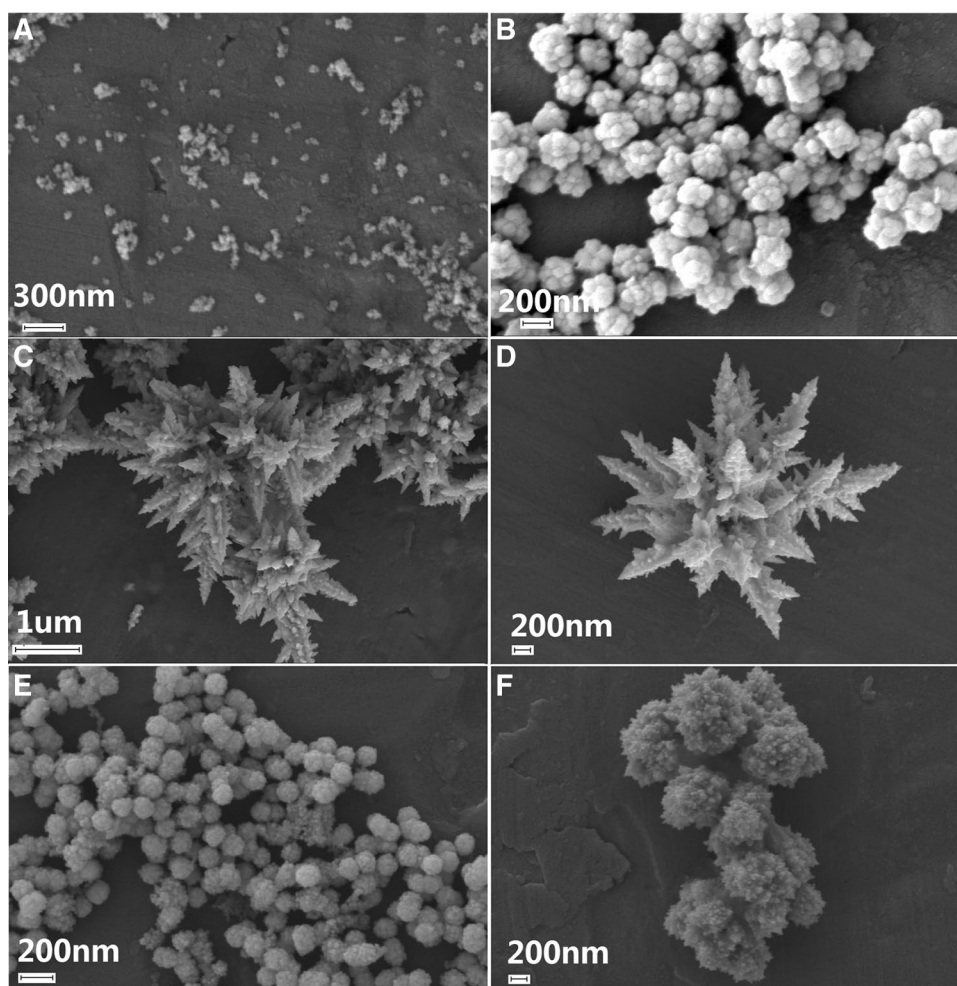


Fig. 1 Powder XRD patterns of GO, snowflake-like CdS, 3D CdS–rGO

Fig. 2 SEM images of CdS prepared without L-aspartic acid (a) and with 1 mmol L-aspartic acid (b), and with 2 mmol L-aspartic acid (c, d), and with 4, 5 mmol L-aspartic acid (e, f)



5 mmol (Fig. 2e, f), the snowflake structure of CdS gradually disappeared. The above experimental results show that the concentration of L-aspartic acid to a large extent affect the morphology of CdS. To our knowledge, the mechanism of CdS growth may relate with the selective adsorption of L-aspartic acid on certain crystal surfaces, and the driving force of this selective adsorption may involve a hydrogen bonding effect, which has been reported previously [26].

At the reaction system temperature of 80 °C, there is no CdS formation in the reactor, which is mainly due to the low decomposition of thiourea under low temperature conditions. As the temperature rises to 100 °C, it can be seen that the products are spherical deposits of uneven size (Fig. 3a). With temperature elevated to 120 °C, it is observed that the size of the spherical stack begins to gradually increase in the Fig. 3b. Continue to improve the reaction temperature to 140 °C, the system appears structured small size flower accumulation (Fig. 3c). When the reaction temperature further increases, the system appears in the structure of the rules of snowflake-like CdS, flower-like accumulation gradually disappeared (Fig. 3d).

Through a basic experiment process and observation above, a suitable mechanism was proposed to explain the formation of snowflake-like CdS. Which is described in Fig. 4. As the temperature and pressure of the system rise to a certain stage, C=S bond of thiourea is gradually broken, S²⁻ ions are slowly released, followed by rapid reaction with Cd²⁺ ions in the solution to produce CdS nanoparticles. At the beginning of the reaction, CdS nanoparticles are produced in small amounts, and L-aspartic acid is effectively adsorbed on the surface of the original CdS nanoparticles, these nanoparticles are then attracted to each other to form small agglomerated particles by hydrogen interaction, then the diffusion controlled growth occurs in the spherical stack, where the surface area decreases during particle fusion and structural rearrangement. With the increase of temperature, thiourea is further decomposed, more and more CdS nanoparticles are synthesized, the amount of L-aspartic acid in some of its crystal surface selective adsorption, these small particles are then contacted by hydrogen interaction and grown in a specific direction towards some of the crystal faces, resulting in this snowflake structure. When

Fig. 3 SEM images of samples prepared at different temperatures: **a** 100, **b** 120, **c** 140, and **d** 180 °C

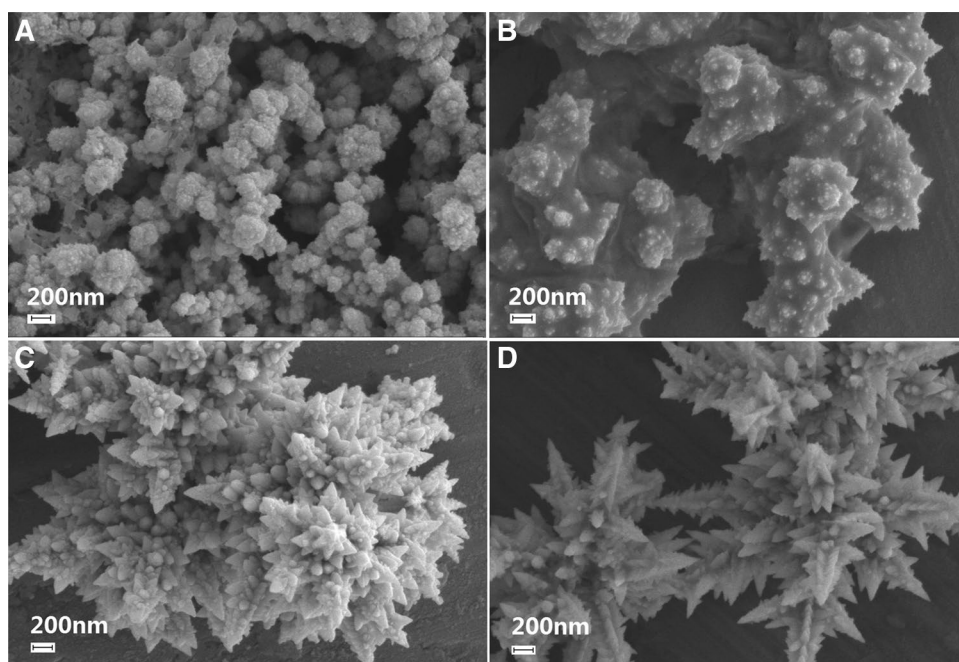
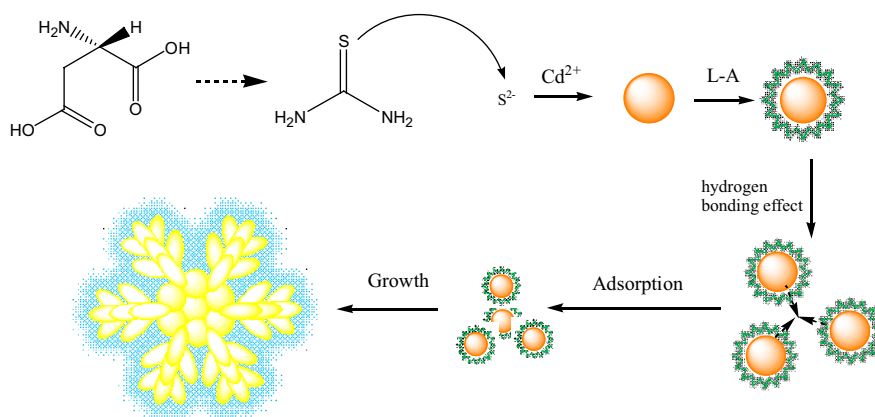


Fig. 4 Schematic illustration for the formation of snowflake-like CdS nanomaterials



the L-aspartic acid is less, it is not enough to adsorb on the surface of CdS and cause simple spherical accumulation. However, L-aspartic acid is added in excess, which can cover all facets of CdS, and the hydrogen interaction leads to the agglomeration of CdS nanoparticles, followed by the growth of large irregular structures.

Figure 5a, b displays the typical TEM images of snowflake-like CdS and CdS-rGO nanocomposites, respectively. TEM image (Fig. 5a) shows that L-aspartic-assisted method for preparation of CdS does generate 3D snowflake-like structure. Figure 5b shows that the rGO film is successfully coated on the surface of the snowflake-like CdS. In addition, main lattice fringe of CdS is clearly distinguished in the HRTEM image (Fig. 5c). The spacing of 0.33 nm can be ascribed to the (002) crystal faces of hexagonal phase CdS, according to the XRD of hexagonal phases in samples.

To detect the state of the rGO nanosheets, the FT-IR spectra of GO and 3D CdS-rGO nanocomposites were obtained. As plotted in Fig. 6, In the spectrum of GO, the peaks at 3400, 1730 and 1050 cm^{-1} are assigned to the -OH stretching vibrations, C=O stretching vibrations and the C-O (alkoxy) stretching vibrations peak, respectively. The bands at around 1220 and 1390 cm^{-1} are indexed to the C-O stretching vibrations in phenolic hydroxyl groups and tertiary C-OH groups, respectively [27]. However, the characteristic peaks of oxygen-containing groups owe to GO are disappeared entirely or weaken greatly in the spectrum of 3D CdS-rGO compared with GO, confirming that GO have been reduced into rGO during the hydrothermal process. There is a new peak located at $\sim 1640 \text{ cm}^{-1}$ emerges, which can be ascribed to the skeletal vibration of the graphene sheets. Two other new characteristic bands at about 1380

Fig. 5 TEM images of snowflake-like CdS (a), 3D CdS-rGO (b), and HRTEM images of 3D CdS-rGO photocatalyst (c)

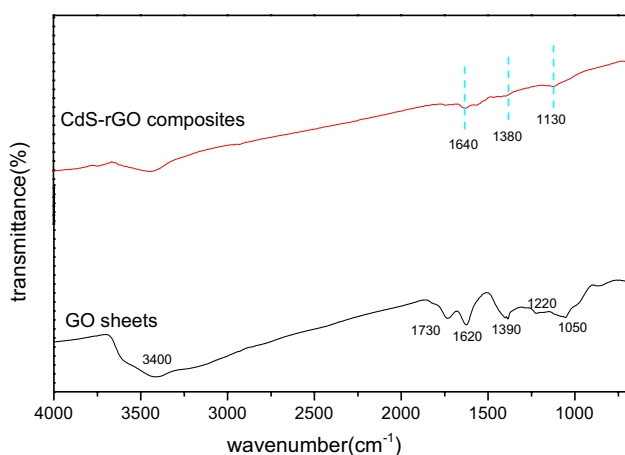
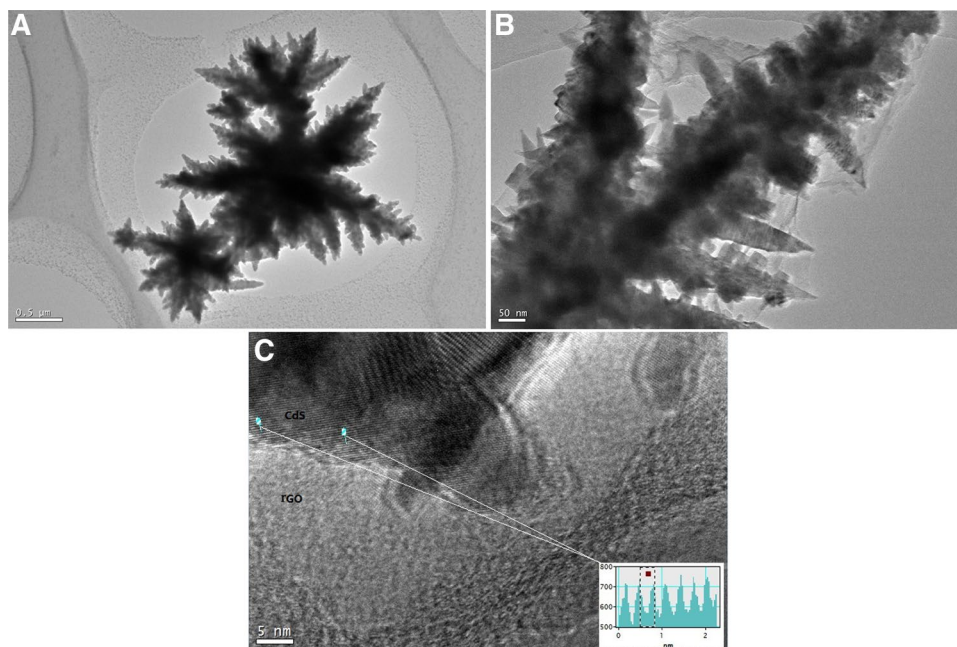


Fig. 6 FTIR spectra of GO, 3D CdS-rGO composites

and 1130 cm^{-1} can be attributed to the Cd-S bond, indicating that the composite photocatalyst is composed of rGO and CdS.

To further characterize the 3D CdS-rGO composite, XPS was employed to gain insight into the surface composition and element analysis of the resulting products (Fig. 7). It can be clearly found in Fig. 7a, the dominant XPS peaks in the survey spectrum of 3D CdS-rGO are assigned to the characteristic peaks of C1s, Cd3d and S2p, indicating the existence of carbon, cadmium and sulfur elements in the sample. Another relatively weak N1s peak in the spectrum of 3D CdS-rGO confirmed the presence of L-aspartic acid. Figure 7b, c show the high-resolution C1s XPS spectra of GO and 3D CdS-rGO. The C1s spectrum of GO could be deconvoluted into three peaks at 284.8, 287.1 and 289.1 eV,

which can be assigned to C-C, C-O and C=O, respectively [28]. For 3D CdS-rGO, the peak intensities of these above oxygen containing functional groups were dramatically reduced, indicating the efficient reduction of most oxygen-containing functional groups in GO during hydrothermal processes. As shown in Fig. 7d, the binding energies of Cd 3d are located at 404.7 and 411.4 eV which can be attributed to Cd 3d_{5/2} and Cd 3d_{3/2}, respectively. And the binding energy is located at 162.2 eV can be attributed the S 2p_{1/2} (Fig. 7e).

The optical properties of pure CdS, snowflake-like CdS and 3D CdS-rGO composites were measured using UV-visible absorption spectra in the wavelength range of 300–700 nm. As shown in Fig. 8, all of the materials show strong light absorption. And the absorption intensity of pure CdS without L-aspartic acid starts to increase rapidly at ca 550 nm. According to the band gap equation:

$E_g = 1239.4/\lambda$, the values of the band gap calculated for pure CdS is 2.26 eV (inset). The light absorption edge gradually shifts toward the visible light region of CdS with L-aspartic acid sample can be seen, and a little red-shift indicates a little decrease in the bandgap energy of the CdS. This also implies that CdS with L-aspartic acid has a smaller band gap. In comparison to pure CdS and snowflake-like CdS, The 3D CdS-rGO composite shows narrower band gap and stronger light absorption in both visible and UV light region. And with the increase of rGO, the absorption of light on the composite showed an increasing trend. This is mainly because that rGO nanosheets introduce a wide light absorption and the possible electronic transition between rGO and CdS [29]. The narrower band-gap and extended light absorption range of

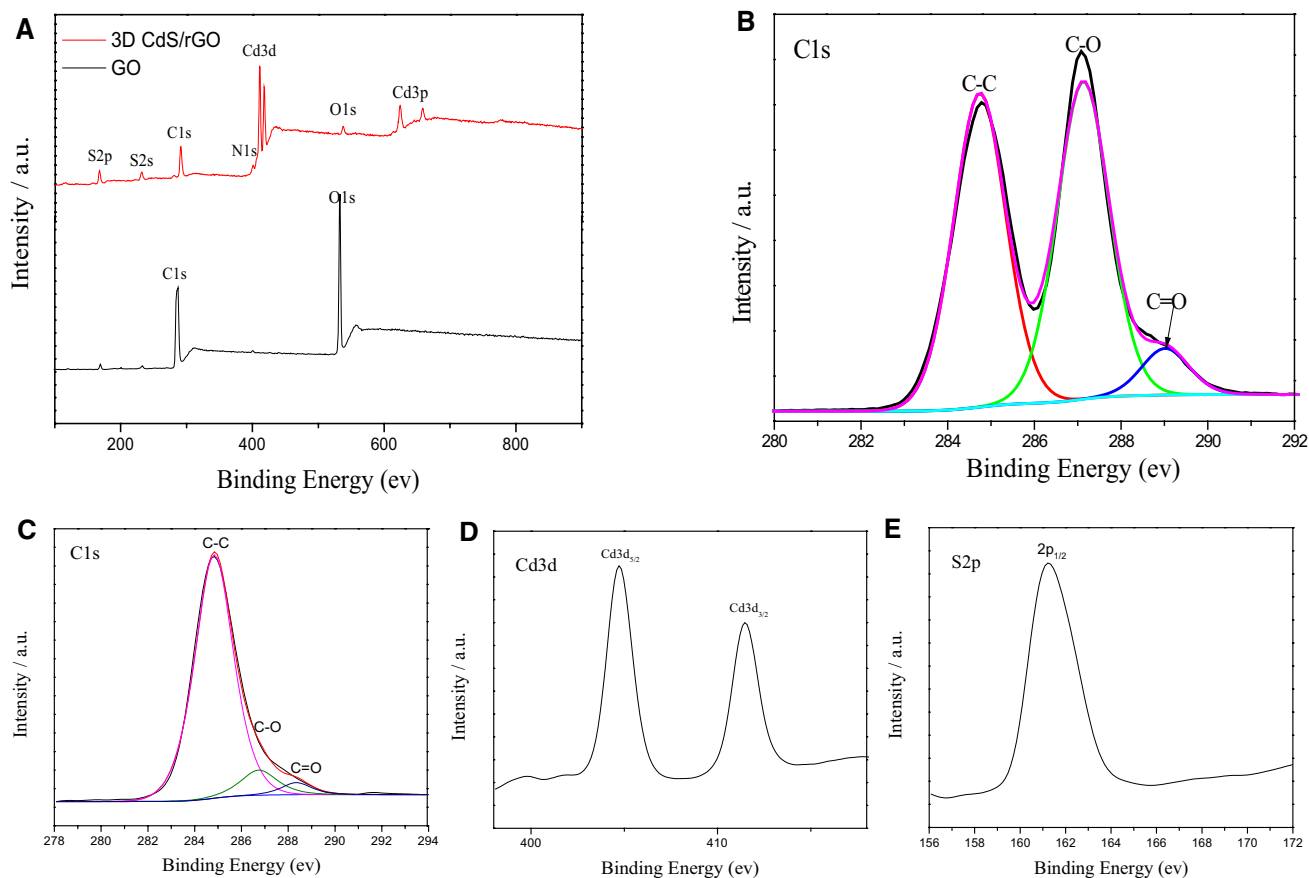


Fig. 7 XPS spectra of GO and 3D CdS-rGO. **a** XPS survey spectra of 3D CdS-rGO and GO, **b** C1s XPS spectrum of GO, **c** C1s XPS spectrum of 3D CdS-rGO, **d** Cd 3d XPS spectrum of 3D CdS-rGO and **e** S 2p XPS spectrum of 3D CdS-rGO

3D CdS-rGO could bring about more efficient utilization of the light, and consequently leading to much enhanced photocatalytic activity.

Photochemical characterization of photocatalyst is mainly depends on the generation of photoinduced electrons, electron-hole pairs separation efficiency and charge carriers transfer. As shown in Fig. 9, the samples were measured on a photoelectrochemical test device under the visible-light irradiation, and a series of electric signals could be obtained with and without irradiation of the 3D CdS-rGO and CdS electrode, The current is drastically increased when the light is on. The initial current density of pure CdS is $0.25 \mu\text{A}/\text{cm}^2$, whereas the current density of the CdS added with L-aspartic acid was higher than that of CdS without L-aspartic acid. This is mainly due to the fact that the photoinduced charge carriers of CdS with L-aspartic acid can be more effectively separated than pure CdS [30, 31]. However, rGO-coated 3D CdS exhibits a stronger photocurrent than pure CdS. This enhanced photoresponse indicates that the photoinduced electrons and holes in the snowflake-like CdS prefer separately transferring to the rGO. As a consequence, the radiative recombination of the electron-hole pairs is hampered

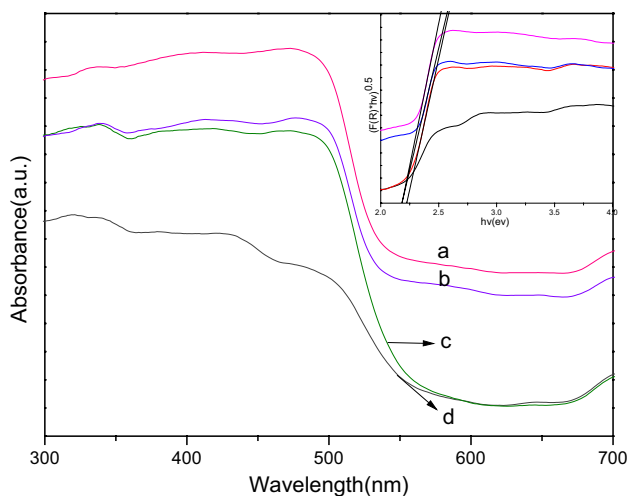


Fig. 8 UV-vis absorption spectra of 3D CdS-rGO (1%) (a), 3D CdS-rGO (3%) (b), snowflake-like CdS (c), pure CdS (d). The derived plots of transformed Kubelka-Munk function versus the energy of light (inset)

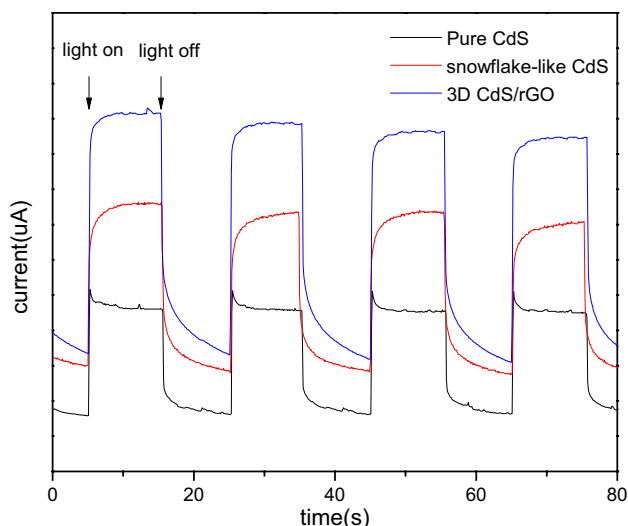


Fig. 9 Transient photocurrents of the pure CdS, snowflake-like CdS and 3D CdS-rGO

and the photocatalytic activity is enhanced significantly for the CdS-rGO photocatalyst.

To compare the photocatalytic activities of pure CdS, snowflake-like CdS and 3D CdS-rGO over time, a photodegradation experiment was carried out using RhB as a model pollutant under simulated sunlight. The evolution of RhB removal rate using the different photocatalysts is shown in Fig. 10a, b. It can be observed that both snowflake-like CdS and 3D CdS-rGO have excellent adsorb ability for dye pollutants. The high adsorption capacity of the composites (snowflake-like CdS 20%) to dye molecules is favorable for the following photodegradation step, which might be due to the non-covalent intermolecular forces [32]. Figure 10a

also shows the degradation rate of RhB over different components of the catalyst under simulated sunlight 140 min irradiation. And there is few change for the concentration of RhB in the absence of any catalyst, indicating that the RhB aqueous solution is fairly stable and scarcely decomposed under visible light. Thus, the self-degradation of RhB is negligible compared to photocatalytic degradation products. Pure CdS exhibits a photodegradation efficiency of (68%), which is mainly due to the rapid recombination of photo-generated electron-hole pairs [33].

However, the snowflake-like CdS exhibit higher photocatalytic efficiency (96%) after loading rGO on its surface (Fig. 9b), indicating that wrapping CdS with rGO sheets can greatly improve the photocatalytic performance of the composites. The enhanced performance can be attributed to rGO an effective electron acceptor, Photogenerated electrons can be quickly transferred from the conduction band (CB) of CdS to the rGO sheet, which facilitates charge separation, suppresses the recombination of electron-hole pairs, and improves the light conversion efficiency of catalysts. Meanwhile, we found that adding different amounts of rGO could alter the photocatalytic activity of the composites. This observation is similar to the findings of previous reports related to rGO-semiconductor composite. The main reason is that a large amount of rGO not only reduces the absorption efficiency, but also affects the light to reach some of the active sites of semiconductor materials [34].

In addition to the activity of photocatalysis, significant photoresistation has been a challenge to hinder the application of cadmium sulfide photocatalysis. Therefore, the stability analysis of cadmium sulfide is essential. In this study, three consecutive RhB degradation cycle tests were carried out by 3D CdS-rGO. Each run was carried out at

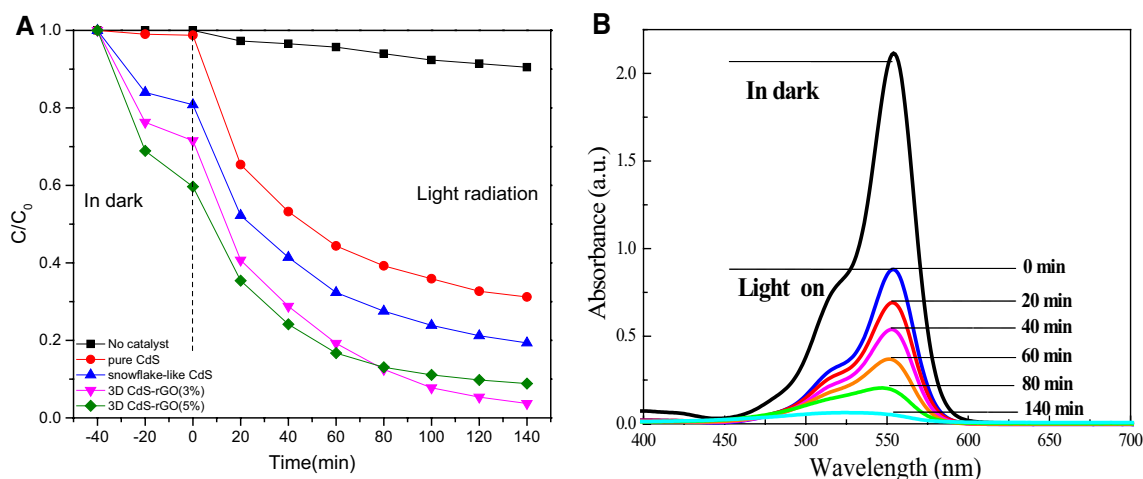


Fig. 10 Photodegradation of methylene blue under simulated sunlight by blank, and pure CdS, snowflake-like, 3D CdS-rGO (3%), and 3D CdS-rGO (5%) (a), the time dependent absorption spectra of RhB

solutions during simulated sunlight irradiation in the presence of 3D CdS-rGO (3%) (b)

the same concentration of 10 mg/L RhB solution, consisting of adsorption and photodegradation processes, respectively. As shown in Fig. 11, the RhB removal rate of the 3D CdS–rGO complex was maintained at 91.8% after three times of repeated use, indicating that the composite catalyst prepared by us had excellent stability and good reproducibility. This may be due to the effect of size change on snowflake-like CdS and good affinity and stable interface contact with reduced graphite oxide.

On the basis of the characterization and experimental data discussed above, a possible photocatalytic mechanism for the degradation of RhB over 3D CdS–rGO composite was illustrated in Fig. 12. Under the visible light irradiation, the electrons in the valence band (VB) of the 3D snowflake-like CdS are excited to the CB, and the same

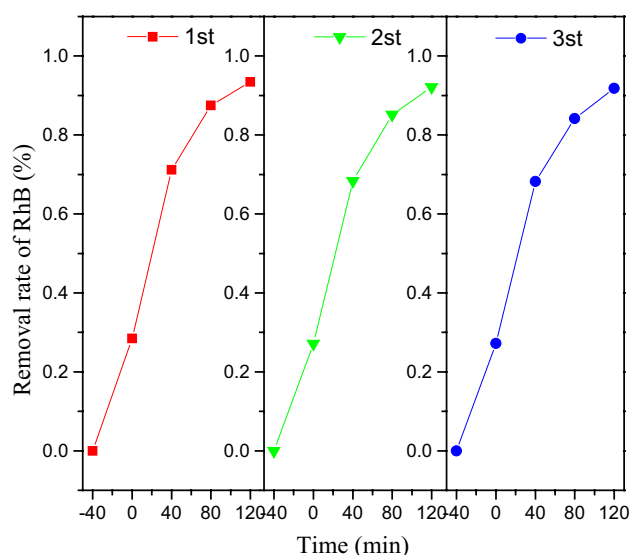
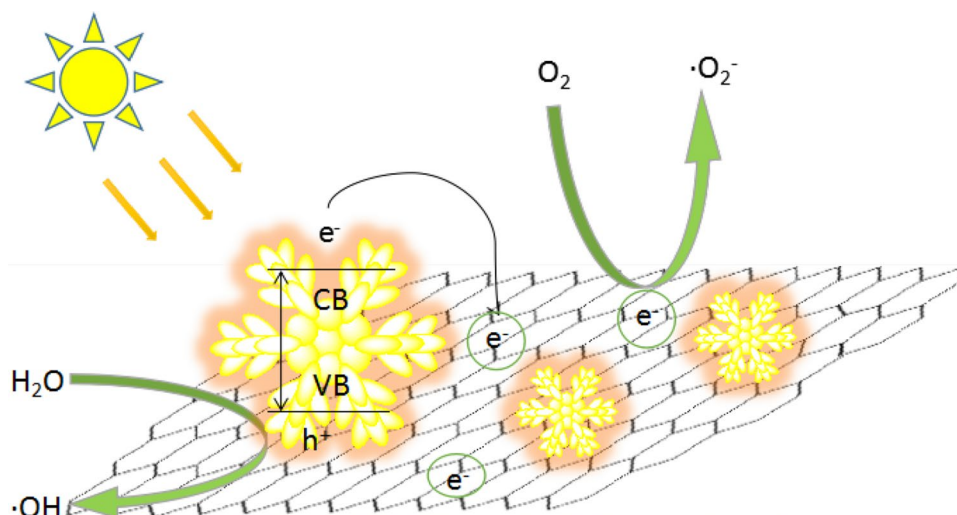


Fig. 11 Recycling test for the removal of RhB by 3D CdS–rGO composite

Fig. 12 The simplified mechanism for the enhanced photocatalytic activity of 3D CdS–rGO composite



amount of holes is generated in VB. Due to the introduction of rGO, the electrons generated by photoexcitation can be transferred to the surface of rGO through the intimate interfacial contact between rGO and snowflake-like. In this process, the lifetime of the photoexcited electrons and holes is prolonged. The photoelectrons transferred to the rGO surface are further captured by dissolved oxygen in the water to form reactive oxygen species, which reacts with water to form hydroxyl radicals ($\cdot\text{OH}$) in the system, electrons transferred to the rGO surface can also react with dissolved oxygen in the solution to produce superoxide anion ($\cdot\text{O}_2^-$). Superoxide anion radicals ($\cdot\text{O}_2^-$) and hydroxyl radicals ($\cdot\text{OH}$) both have a strong ability to oxidize and react with organic molecules in the solution to produce CO_2 , H_2O , and other intermediates. At the same time, the separated holes are consumed to oxidize the dye molecules directly on one hand. On the other hand, holes on the VB of snow-like CdS can react with H_2O or hydroxyl ions (OH^-) adsorbed on the surface of the catalyst to form hydroxyl radicals ($\cdot\text{OH}$), which are involved in the degradation of organic dyes. rGO plays an important role in the overall reaction system, firstly, rGO can be used as electron carrier and transporter to accept and transfer photoelectrons produced by visible light irradiation on 3D snow-like CdS surface, inhibit the rapid recombination of electron holes, and enhance the photocatalytic activity. Secondly, rGO possesses great adsorption capacity for organic dye molecules, mainly due to the strong π - π interaction between them. In addition, rGO also plays a role in protecting the 3D snowflake-like CdS structure and reducing the corrosion of light, and thereby improving the stability of the photocatalyst.

4 Conclusions

We have successfully fabricated a novel chemically cross-linked 3D CdS–rGO composite photocatalyst with enhanced sunlight-driven photocatalytic activity and stability are fabricated via a facile hydrothermal method. Based on SEM observation, a simple snowflake-like CdS nanostructure growth mechanism was proposed. L-Aspartic acid was found to be effectively adsorbed on the surface of the original CdS nanoparticles which prevent the simply agglomeration of CdS. 3D CdS–rGO shows excellent visible light absorption and enhanced photocurrent mainly due to the special morphology of CdS and the introduction of rGO, which reduces the rapid recombination of electrons–holes and thus increasing the catalytic activity of the catalyst. It is found that composite also reveals enhanced degradation rate and high stability during photocatalytic degradation of organic pollutants. We believe that this kind of photocatalyst will have a promising prospect in efficiently removing the organic contaminants from water. Furthermore, the fabrication method described in this study is simple and can be used to develop other 3D nanomaterials integrated with graphene for creating more 3D composites with fascinating properties for a variety of applications.

Acknowledgements The authors were greatly appreciated to the National Natural Science Foundation of China (51262027), the Natural Science Foundation of Gansu Province (0803RJZA009), Science and Technology Tackle Key Problem Item of Gansu Province (2GS064-A52-036-08), Gansu Key Laboratory of Polymer Materials (ZD-04-14) and the support from the fund of the National Key Laboratory of Solidification Technology (SKLSP201754) for its financial support.

References

1. T. Hisatomi, J. Kubota, K. Domen, *Chem. Soc. Rev.* **43**, 7520–7535 (2014)
2. H. Ramezanalizadeh, F. Manteghi, *J. Photochem. Photobiol. B* **338**, 60–71 (2017)
3. M. Hussaina, P. Akhter, G. Saracco, N. Russo, *Appl. Catal. B* **170**, 53–56 (2015)
4. Y. Wang, Z. Mo, C. Zhang, P. Zhang, R. Guo, H. Gou, X. Wei, *J. Ind. Eng. Chem.* **32**, 172–177 (2015)
5. Q. Wang, J. Li, N. An, Y. Bai, X. Lu, J. Li, W. Shanguan, *Int. J. Hydrogen Energy* **38**, 10761–10767 (2013)
6. S. Liu, Z. Chen, N. Zhang, Z.R. Tang, Y.J. Xu, *J. Phys. Chem. C* **117**, 8251–8261 (2013)
7. D. Ghosh, S. Mondal, S. Ghosh, A. Saha, *J. Mater. Chem.* **22**, 699–706 (2012)
8. G. Wu, Y. Wang, K. Wang, A. Feng, *RSC Adv.* **6**, 102542–102548 (2016)
9. H. Wu, G. Wu, Y. Ren, X. Li, L. Wang, *Chem. Eur. J.* **22**, 8864–8871 (2016)
10. G. Wu, H. Wu, K. Wang, C. Zheng, Y. Wang, A. Feng, *RSC Adv.* **6**, 58069–58076 (2016)
11. Q. Wu, X. Chen, P. Zhang, Y. Han, X. Chen, Y. Yan, S. Li, *Cryst. Growth Des.* **8**, 3010–3018 (2008)
12. A. Kudo, Y. Miseki, *Chem. Soc. Rev.* **38**, 253–278 (2009)
13. G. Dukovic, M.G. Merkle, J.H. Nelson, S.M. Hughes, A.P. Alivisatos, *Adv. Mater.* **20**, 4306–4311 (2008)
14. Y. Shemesh, J.E. Macdonald, G. Menagen, U. Banin, *Angew. Chem.* **123**, 1217–1221 (2011)
15. A. Cao, Z. Liu, S. Chu, M. Wu, Z. Ye, Z. Cai, Y. Chang, S. Wang, Q. Gong, Y. Liu, *Adv. Mater.* **22**, 103–106 (2010)
16. D.R. Baker, P.V. Kamat, *Adv. Funct. Mater.* **19**, 805–811 (2009)
17. F. Akbar, M. Kolahdouz, S. Larimian, B. Radfar, H.H. Radamson, *J. Mater. Sci.: Mater. Electron.* **26**, 4347–4379 (2015)
18. S. Stankovich, R.D. Piner, X. Chen, N. Wu, S.T. Nguyen, R.S. Ruoff, *J. Mater. Chem.* **16**, 155–158 (2006)
19. G. Wu, Y. Cheng, Z. Wang, K. Wang, A. Feng, *J. Mater. Sci.: Mater. Electron.* **28**, 576–581 (2017)
20. X. Wang, B. Yuan, Z. Xie, D. Wang, R. Zhang, *J. Colloid Interface Sci.* **446**, 150–154 (2015)
21. G. Zhao, Z. Mo, P. Zhang, B. Wang, X. Zhu, R. Guo, *J. Porous Mater.* **22**, 1245–1253 (2015)
22. H. Gao, Z. Mo, Y. Wang, X. Niu, Z. Li, *J. Mater. Sci.: Mater. Electron.* **28**, 14543–14553 (2017)
23. D.C. Marcano, D.V. Kosynkin, J.M. Berlin, A. Sinitskii, Z. Sun, A. Slesarev, J.M. Tour, *ACS Nano* **4**, 4806–4814 (2010)
24. Y. Wang, Z. Mo, P. Zhang, C. Zhang, L. Han, R. Guo, R. Hu, *Mater. Des.* **99**, 378–388 (2016)
25. J. Liu, H. Bai, Y. Wang, Z. Liu, X. Zhang, D.D. Sun, *Adv. Funct. Mater.* **20**, 4175–4181 (2010)
26. X. Zhang, Q. Zhao, Y. Tian, Y. Xie, *Cryst. Growth Des.* **4**, 355–359 (2004)
27. L. Liu, M. An, P. Yang, J. Zhang, *Sci. Rep.* **5**, 9055–9064 (2015)
28. P. Huo, M. Zhou, Y. Tang, X. Liu, C. Ma, L. Yu, Y. Yan, *J. Alloy. Compd.* **670**, 198–209 (2016)
29. X.Y. Zhang, H.P. Li, X.L. Cui, Y. Lin, *J. Mater. Chem.* **20**, 2801–2806 (2010)
30. M.Q. Yang, Y. Zhang, N. Zhang, Z. R. Tang, Y.J. Xu, *Sci. Rep.* **3**, 3314–3321 (2013)
31. X. Zhang, Y. Li, J. Zhao, S. Wang, Y. Li, H. Dai, X. Sun, *J. Power Sources* **269**, 466–472 (2014)
32. X. Wang, H. Mao, Y. Shan, *RSC Adv.* **4**, 35614–35619 (2014)
33. Q. Li, B. Guo, J. Yu, J. Ran, B. Zhang, H. Yan, J.R. Gong, *J. Am. Chem. Soc.* **133**, 10878–10884 (2011)
34. L. Xu, F. Zhang, X. Song, Z. Yin, Y. Bu, *J. Mater. Chem. A* **3**, 5923–5933 (2015)